# Microwave Technique for Liquid Water Detection in Icing Applications

**Author, co-author (Do NOT enter this information. It will be pulled from participant tab in MyTechZone)**

Affiliation (Do NOT enter this information. It will be pulled from participant tab in MyTechZone)

## Abstract

The partial melting of ingested ice crystals can lead to ice accretion in aircraft compressors, but accurately measuring the relatively small fraction of liquid water content in such flows is challenging. Probe-based methods for detecting liquid water content are not suitable for deployment within turbofan engines, and thus alternatives are sought. Recent research has described approaches based on passive microwave sensing. We present here an approach based on active microwave transmission and reflection, employing a vector network analyzer. Utilization of both transmission and reflection provides additional data over and above emission or transmission only, and permits a more controllable environment than passive sensing approaches. The paper specifically addresses the question of whether such an approach is viable within the context of representative icing wind tunnel and engine flow conditions. A quasi-thermal equilibrium approach is presented herein to estimate the melting ratio during microwave analysis of samples at 0 °C. Experimental results using microwaves in the 2.45GHz region are presented, and post-processing methods investigated. This is followed by an investigation of detection limits for ice accretion in the sub-gram range. The results indicate the potential of the technique, with a number of avenues evident for further research.

## Introduction

Wind tunnel experiments can contribute to our understanding of the ice crystal icing problem but an accurate knowledge of the flow conditions being produced by any wind tunnel is essential for meaningful interpretation and analysis of data. The ice crystal icing problem is complex, so being able to quantify flow conditions accurately is critical for development of reliable modelling techniques.

One variable that is particularly important in the ice crystal icing problem is the melting ratio ($MR$) which specifies the ratio of Liquid Water Content (LWC) to Total Water Content (TWC). Conditions leading to the most rapid development of accretion typically occur for $MR \sim 0.1$, whereas very little accretion occurs for $MR \sim 0$ and $MR \sim 0.25$ [1, 2]. Therefore, being able to specify the value of $MR$ with a certainty of 0.01 or better would be useful. However, such a level of accuracy is a challenge because probe methods that attempt to distinguish LWC from the TWC typically require extensive characterization, and even then, uncertainties in the particle capture / measurement efficiency for the two phases tend to persist. While it may be possible to accurately measure the TWC with an isokinetic probe [3], discrimination between liquid and solid phases typically requires Nevzorov-like probes which rely on differences in liquid and solid particle impacts (liquid particles tend to stick, whereas ice particles tend to bounce/shatter) which generate different surface heat transfer signatures [4, 5].

Microwaves may offer a viable alternative for the discrimination between solid and liquid water content. Microwave techniques have previously been applied to the measurement of liquid and solid water in different applications. For example, an ice slurry was considered in [6], whereas steam quality measurements were performed in [7]. Trapp et al. [8] reported on a passive radiometric sensor for detecting the presence of ice accretion, which used the frequency range 8.2-12.4 GHz. Faulkner et al [9] improved upon this with a more compact sensor and measurement results. This approach is based around a Dicke radiometer which measures power alternately between the object under test and the background radiation. This works to mitigate against background noise and reduce the influence of gain fluctuations. The use of the 10.65 GHz ITU passive sensing band for this work is advantageous.

The approach we are proposing uses an active measurement, based on a VNA (Vector Network Analyzer). Such a technique does not appear to have been investigated in the context ice crystal wind tunnel experiments. The non-intrusive microwave technique for measurement of liquid water content is appealing because it will not have the uncertain capture efficiency of probe-based techniques.

## Approach for Microwave Measurements

The use of microwave radiation in the 1-10 GHz frequency range has been reported for a number of practical applications. For example, grain moisture levels were estimated with high precision in [10], with single grains able to be accurately measured within a microwave resonator. Steam quality indexes were shown to be able to be determined using microwave techniques [7]. Here, a Vector Network Analyzer (VNA) was used to determine the $S_{21}$ parameter, and it is shown that the permittivity of the mixture can be related to the volume mixing ratios.

Central to our proposed approach using microwaves is the critical observation that the dielectric properties of liquid water and ice are somewhat different [11], especially at microwave frequencies [12]. Furthermore, at 0 °C water and ice can coexist in thermal equilibrium [11]. This second observation, while central to our proposed calibration approach presented in this paper, may not strictly apply in future wind tunnel experiments or in the engine environment where particles of liquid water and ice may have different temperatures. Nevertheless, these physical attributes have proven to be useful in the measurement of ice fraction in ice slurries [6]. Although a different problem domain, fully liquid water content with ice incorporated as a solid, [6] demonstrates clearly that electromagnetic (EM) attenuation at radio frequencies (RF) may be used to discriminate between ice and water, and indeed measure the proportion of ice. At ~2.45 GHz, [6] noted a water/ice attenuation ratio of approximately 70. Furthermore, the complex index of refraction is directly proportional to wave absorption. The physical mechanisms involved are further discussed in [6].

In microwave measurements, it is usual to measure the power scattering or S parameters, defined as

$$\boldsymbol{S} = \begin{pmatrix} S_{11} & S_{12} \\ S_{21} & S_{22} \end{pmatrix}$$

These are complex-valued quantities, measured using a vector network analyzer (VNA). The transmit and receive antenna ports are treated as a two-port Device Under Test (DUT), and calibrated according to standard SOLT (Short-Open-Load-Through) techniques [13]. The automatic calibration approach is standard and widely used, and was introduced by Evans [14] with further refinements by Kruppa and Renmark [15].

We experimented with direct use of the transmission S parameters ($S_{21}$ & $S_{12}$), as well as conversion to transmission ($T$) and reflection ($R$) coefficients. These are related via

$$S_{11} = \frac{(1-T^2)\,R}{1-R^2T^2} \tag{1}$$

$$S_{21} = \frac{(1-R^2)\,T}{1-R^2T^2} \tag{2}$$

The reverse, to determine the transmission and reflection coefficients, is performed using the Nicholson-Ross-Weir method [16, 17]

$$X = \frac{1-S_{21}^2+S_{11}^2}{2\,S_{11}} \tag{3}$$

$$R = X \pm \sqrt{X^2-1} \tag{4}$$

$$T = \frac{S_{11}+S_{21}-R}{1-(S_{11}+S_{21})R} \tag{5}$$

The sign ambiguity in $R$ is resolved by choosing ± such that $|R| \leq 1$.

## Apparatus and Methods

### *Wind Tunnel*

The icing wind tunnel facility that will be used in the present work is illustrated in Figure 1; it is the recently-developed icing wind tunnel at the University of Southern Queensland and the test section cross section dimensions are $305 \times 305$ mm. The test section of the wind tunnel is fabricated from clear acrylic sheets. A bell-mouth is positioned immediately upstream of the test section, and an icing jet nozzle of diameter $D_j = 170$ mm is positioned on the centerline, at the upstream edge of the test section. Flow speeds of around $u_j =$ 40 m/s can be generated in the facility and the target total water content conditions are up to approximately $TWC = 10$ g/m$^3$.

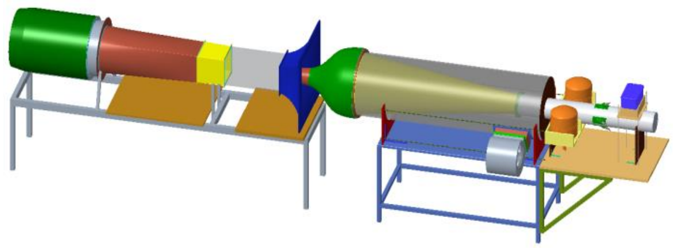

Figure 1. Illustration of the USQ icing wind tunnel facility. The left-hand portion of the facility is conventional subsonic wind tunnel duct; the right-hand portion of the facility is the icing jet generator. General direction of the flow is from right to left in this view.

### *Microwave hardware*

For the initial experiments reported here, the vector network analyzer (VNA) transmit and receive antennas were secured to a simple frame that straddled a water sample enclosure as illustrated in Figure 2. Eventually, we plan to position the transmit and receive antennas on either side of the wind tunnel test section to measure the transmission coefficient of the flow from the icing nozzle. However, before progressing to the wind tunnel configuration, laboratory bench-top experiments have been performed to ascertain the viability of the planned wind tunnel experiments.

The VNA is a PicoTechnology (https://www.picotech.com/) model 106 two-port VNA capable of measuring all four S parameters. The resolution bandwidth was set to 10 Hz with a frequency span of 2350-2600 MHz. One sweep of this range at this bandwidth takes just over 60 seconds. The output power used in the present experiments was - 3 dBm corresponding to 0.5 mW, but the VNA has the capacity to be operated at +6 dBm.

Antennas are 50 mm monopole soldered directly to a standard BNC connector. The container for both transmitter and receiver is approximately 70 mm in diameter and 100 mm long. It is noted that this arrangement is not optimized to the frequency used, since the actual frequency or frequency band which best exhibits the liquid/solid discrimination under these conditions is part of the current investigation.

The water samples are fully enclosed in a PVC dish of diameter 90 mm with suitable 4-wire shielded cable egress for PT100 sensors. The temperature transducers are PT100 type from Omega Engineering (https://www.omega.com/) with calibration from resistance to temperature performed in MATLAB® using the Callendar-Van Dusen equation. These are certified to IEC 60751 Class B with accuracy +/- 0.3 °C. Each PT100 is measured using a 4-wire resistance connection (probe and sense wires), measured with Rigol DM3058 (5 ½ digit) and DM3068 (6 ½ digit) DMMs (https://www.rigolna.com/). These are connected via USB to a VISA instrument driver, which is called from a C program. This in turn is called from MATLAB to take temperature samples every 2 seconds.

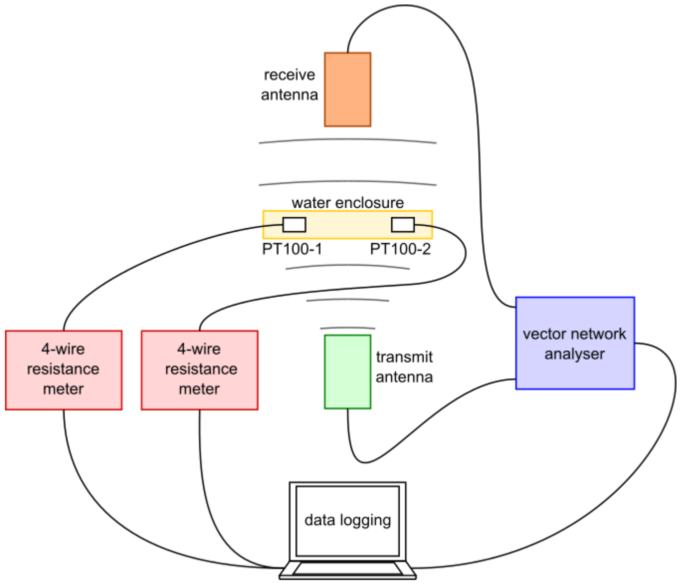


Figure 2. Illustration of apparatus used for assessment of microwave detection of liquid water-ice mixtures.

### *Methods*

Experiments were performed through the following sequence. (i) Remove the enclosure from the microwave bench-top apparatus; (ii) Deliver the required mass of water to the enclosure; (iii) Freeze the enclosure plus water in a separate freezer unit; (iv) Re-install the enclosure within the laboratory bench-top apparatus and commencing the data logging. The mass of water that was frozen in the enclosure dictated the required duration of the experiments: several hours were required to complete the melting process when the largest water masses were used, whereas the heat-up process was completed within about half an hour when no water was used.

Experiments were performed for 3 cases: (1) 28 grams of water frozen within the enclosure; (2) no water was added to the frozen enclosure; and (3) 0.8 grams of water in the form of a spray was frozen.

Two broad categories of analysis present themselves in microwave sensor systems: active and passive. In the passive sensor case, EM waves emanating from the material under test are analyzed over a broad frequency range. This of course depends on natural emissivity, and in effect measures the microwave equivalent temperature of the material. The disadvantage with this approach is that the change in emissivity for a given change in the target parameter may be negligible, or at least, below the noise measurement threshold. Active analysis, however, irradiates the target material with RF waves of one frequency, or a chosen range of frequencies, and records either or both of the transmission $T$ and reflection $R$. These may then be converted into either complex permittivity or complex index of refraction. Generally, using the VNA approach, $T$ and $R$ are not measured directly, but rather via the microwave scattering parameters. One key advantage of active analysis is that a synchronous signal (the transmitted signal) is available for correlating with the received signal at the receiver.

Within the domain of active analysis, two approaches have been reported in the literature [18]. The transmission techniques utilize signal attenuation and signal phase shift, usually derived from $S$ parameters. An alternative active technique is resonance analysis wherein shift in resonance frequency, together with change in resonance peak bandwidth, are measured. The change in resonance approach is most suited to situations where the material under test is able to be confined within a microwave resonator waveguide, so that the change in resonance characteristics are determined directly. This approach does not lend itself to the present scenario, as containment within a waveguide is not feasible due to the nature of the compressor flow. This leaves the transmission/reflection approach, with the $S$ parameters measured transversally to the flow.

The choice of operating frequency was conjectured to be somewhere in the range of the conventional microwave oven, around 2.45 GHz. This range has several practical advantages. First, the frequency is not overly difficult to generate, nor is antenna design complicated, when compared to frequencies above 10 GHz where the dipole nature of the water molecule exhibits substantially higher RF artifacts. Secondly, the physical antenna size – being related directly to the wavelength, is relatively constrained. One-half wavelength at this frequency is approximately 60 mm. The precise frequency range(s) to be employed is still a matter of investigation.

## Results

### *Thermal performance of enclosure*

Temperature measurements from the two platinum resistance thermometers for an experiment with 28 grams of water frozen in the enclosure are presented in Figure 3. The initial temperature of the frozen water was around -17 °C at the time data logging commenced. The temperature of the ice increased in an approximately linear manner until the melting point was reached after a period of about 10 minutes. A period of approximately two hours of constant temperature was then registered, and during this time, the water transitioned from a fully-frozen state to a fully liquid state. At the end of the constant temperature period, the temperatures registered by the two thermometers increased, and approached the ambient temperature of the laboratory in a nonlinear manner.

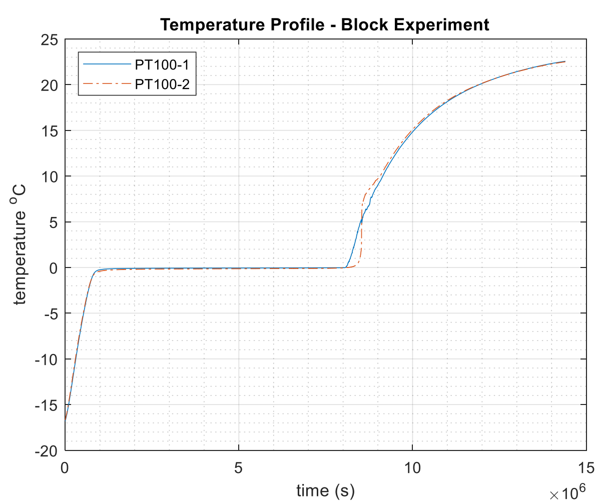


Figure 3. Temperatures measured by the two thermometers (PT100-1 and PT100-2) during an experiment with 28 grams of water in the enclosure.

The rate of heat transfer $\dot{Q}$ (units of W) into the ice and enclosure (for $< 0$ ℃) can be modelled in a lumped thermal capacity form as,

$$\dot{Q}_{T<0} = (m_i c_i + m_e c_e)\left(\frac{d\theta}{dt}\right)_{T<0} = U\,A\,\theta \qquad (6)$$

where $m_i$ and $c_i$ are the mass (kg) and the specific heat (J/kgK) of the ice, $m_e$ and $c_e$ are the mass (kg) and the specific heat (J/kgK) of the enclosure, $\theta = T_{amb} - T$ (°C) is the temperature difference between the ambient laboratory environment and the sample/enclosure, $t$ is the time (s), $U$ (W/m$^2$.°C) is the overall convective heat transfer coefficient, and $A$ (m$^2$) is the surface area of the enclosure. Integrating Equation (6) relative to some reference state (subscript 1) enables us to write

$$\ln\frac{\theta}{\theta_1} = \frac{-UA}{m_i c_i + m_e c_e}\,(t - t_1) \qquad (7)$$

Thus, when the temperature difference $\theta$ is plotted on a log-axis, the slope of this line is given by

$$s_{solid} = \frac{-UA}{m_i c_i + m_e c_e} \qquad (8)$$

As shown in Figure 4, a straight line was fitted to the logarithm of the temperature data in the region between 200 and 700 seconds, corresponding to the period when the water was solid ice but warming up with the heat transfer from the laboratory environment. The slope of the straight line (in the region 0 to 5000 seconds) shown in Figure 4 gives $s_{solid} = -0.705 \times 10^{-3}$ s$^{-1}$.

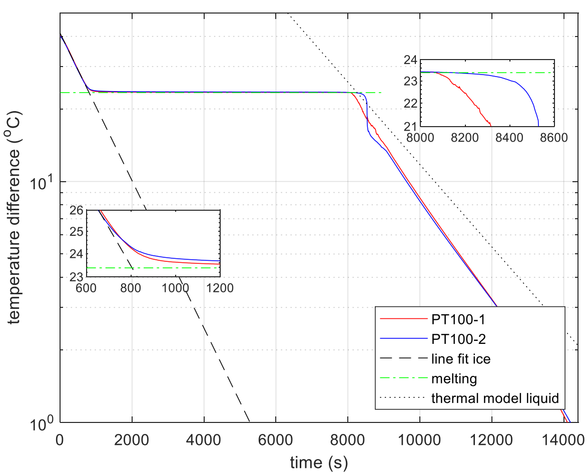


Figure 4. Temperature variation with time for the apparatus operated with $m_i = m_f = 28$ g. Temperature difference is $\theta = T_{amb} - T$ with $T_{amb} = 23.4$ °C.

If there is thermal equilibrium between the water and the enclosure during the period when the sample is actually melting, then the convective heat transfer is providing the energy to melt the ice only this heat transfer can be expressed as

$$\dot{Q}_{T=0} = h_{if}\frac{dm_l}{dt} = U\,A\,\theta \qquad (9)$$

where $h_{if}$ is the latent heat of fusion for the water (taken as $h_{if} = 333.6 \times 10^3$ J/kg), and $m_l$ is the mass of the liquid water being produced during the melting process. Since the temperature difference $\theta$ will remain constant during the melting process, the rate of production of the liquid phase will be constant if thermal equilibrium conditions prevail. Therefore, if the period over which melting occurs can be defined from the experiments as $\Delta t_{melt}$, and the total mass of the water is known either prior to the commencement of the melting $m_i$ or after the melting is completed $m_f$, the melting rate can be defined

$$\frac{dm_l}{dt} = \frac{m_i}{\Delta t_{melt}} = \frac{m_f}{\Delta t_{melt}} \qquad (10)$$

Based on the timing of the departure of the temperature data from the line-fit for the frozen conditions shown in Figure 4, the onset of mixed phase conditions occurred at $700 \pm 30$ seconds, however, it was not until about 900 seconds that both PT100s were within 1 °C of the melting temperature. There was even more uncertainty in the timing of the transition from the mixed phase conditions into the fully-liquid phase conditions. PT100-1 departs from the melting temperature quite rapidly at around $8060 \pm 30$ seconds as shown in Figure 4, but PT100-2 initially departs from the melting temperature in a more gradual manner. There is also about 300 seconds between when PT100-1 and -2 achieve a temperature that is 1 °C higher than the melting temperature. Furthermore, it is not until about 9000 seconds that the two PT100s give temperature values that are within 1 °C of each other. For the initial and final times of the melting period we take $t_{init} = 800 \pm 100$ s and $t_{final} = 8500 \pm 500$ s, so that $\Delta t_{melt} = 7700$ s $\pm\, 7$ %.

For the present experiment with $m_i = m_f = 28$ grams, we therefore have $\dot{m}_l = 3.64 \times 10^{-6}$ kg/s. When this figure is combined with $\theta = 23.4$°C and the value of $h_{if}$ as per Equation (10), we now have the value of $U\,A = 51.8 \times 10^{-3}$ W/°C. Combining this value with Equation (8) and the fitted slope of the line $s_{solid}$, and the specific heat of the ice ($c_i = 2108$ J/kg.°C) we find $m_e c_e = 14.6$ J/°C.

We can write the temperature change in the fully-liquid region as

$$\ln\frac{\theta}{\theta_2} = \frac{-UA}{m_f c_f + m_e c_e}\,(t - t_2) \qquad (11)$$

which is essentially the same as Equation (7) but with the subscript $i$ which referred to the ice state changed to subscript $f$ to refer to the liquid state, and a new reference condition denoted by the subscript 2. The slope of the log-temperature-difference line in the liquid region is therefore

$$s_{liquid} = \frac{-UA}{m_f c_f + m_e c_e} \qquad (12)$$

Since we have the values of $UA$ and $m_e c_e$ defined from $s_{solid}$ and the melting period, and we can also take the specific heat of the liquid water as $c_f = 4187$ K/kg.C, we can calculate the slope of the liquid line as $s_{liquid} = -0.394 \times 10^{-3}$ s$^{-1}$. The slope of such a line is shown in Figure 4 (represented by the dots) and it is seen to be shallow relative to the experimental data in the liquid region.

The rate of production of the liquid water during the phase change was determined from the experimental data to be $\dot{m}_l = 3.64 \times 10^{-6}$ kg/s, and combining this value with Equation (9) gives $\dot{Q}_{T=0} = 1.2$ W, which is the rate of convective heat transfer from the laboratory during the melting process. The microwave power used in the present experiments was 0.5 mW, which is more than three orders of magnitude smaller than the convective heat transfer. Therefore we conclude that the fraction of microwave power that is absorbed by the sample will have no detectable impact on the outcome of the experiments.

The recorded temperature histories during period between 700 and 900 seconds near the start of the melting process, and the period between 8000 and 9000 seconds towards the end of the melting indicate that departures from thermal equilibrium did occur. We can assess the significance of such possible non-equilibrium effects on the specification of the melting ratio through analysis of the uncertainties. Had conditions of thermal equilibrium prevailed throughout the melting period, the melting ratio can be expressed as a linear function of time

$$MR = \frac{t - t_{init}}{t_{final} - t_{init}} \tag{13}$$

Based on Equation (13) and a specification of an uncertainty in $t_{init}$ as $\delta t_{init} = \pm 100$ s, and uncertainty in $t_{final}$ as $\delta t_{final} = \pm 500$ s, we can propagate these uncertainties to the melting ratio as

$$\delta MR = \left[ \left( \delta t_{init} \frac{\partial MR}{\partial t_{init}} \right)^2 + \left( \delta t_{init} \frac{\partial MR}{\partial t_{init}} \right)^2 \right]^{\frac{1}{2}} \tag{14}$$

Results from Equation (14) are presented in Figure 5 for melting ratios up to 0.3. As we are primarily concerned with maximum melting ratio values of $MR \approx 0.2$, the uncertainties in the melting ratio that arise from possible non-equilibrium effects are $\delta MR \leq \pm 0.018$.

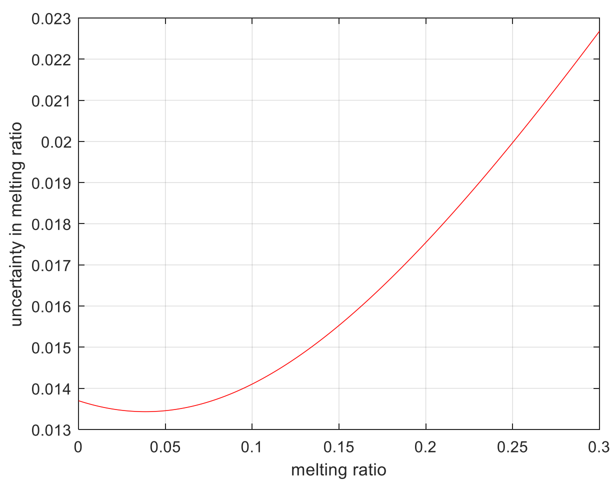


Figure 5. Melting ratio uncertainty for experiments with 28 grams of water.

## *Microwave results*

### Apparatus with large water mass

Initial experiments focused on determining the microwave parameters for a larger (~30 g) water mass, for which the temperature profile could be accurately measured. The goal was to ascertain the measurement uncertainty and likely behavior of the $S$ parameters, and any derived parameters such as transmission and reflection.

Figure 6 shows the path of the derived transmittance parameter $T$ over the complete temperature profile as shown earlier in Figure 3. The path trajectory from ice, through the solid-liquid transition period, eventually to all-liquid, is shown. The axes are the real and imaginary components of the transmission. In operation within the turbine, the path is naturally the reverse – from liquid through to solid, and thus the transition region, and especially the entry to the transition region, is of interest. The initial deviation from the localized liquid area is quite pronounced, with the trajectory following a predictable path towards the ice region.

Two other characteristics are of note. The first is that the measurement points in the complex $T$ plane show a nonlinear step as the linear time step progresses. This is one possible avenue for determining deviation from liquid. The second observation is that the all-ice region is approximately parallel to the transition path, and occurs once the end of the transition path is encountered.

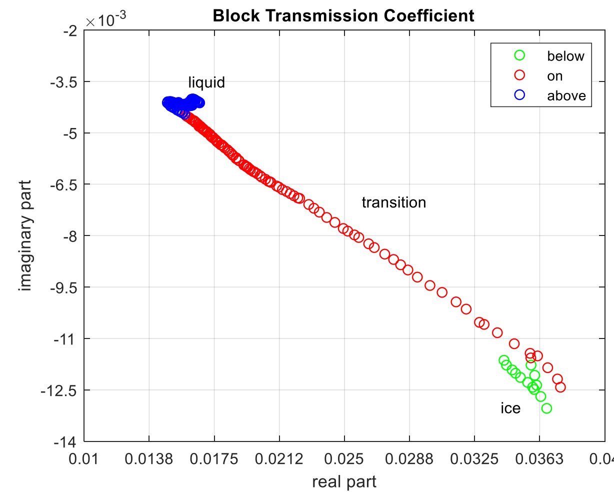


Figure 6. Transmission coefficient for 28 grams of water. Results color-coded according to temperature: 'below' ($T < 0$ °C); 'on' ($T \approx 0$ °C); 'above' ($T > 0$ °C).

### Low-mass and dry apparatus

Next, a benchmark for both a low-mass (< 1g) and dry apparatus is investigated. The temperature profile for the dry apparatus is shown in Figure 7, with the temperature profile for the <1g water spray shown in Figure 8. Of note is the slight deviation of one temperature sensor from the other in the spray experiment. This is thought to be due to ice formed around one of the sensors, but not the other.

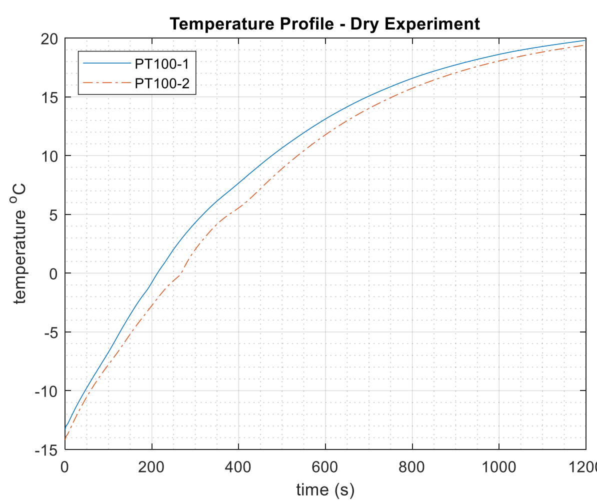


Figure 7. Temperature history for dry apparatus experiment.

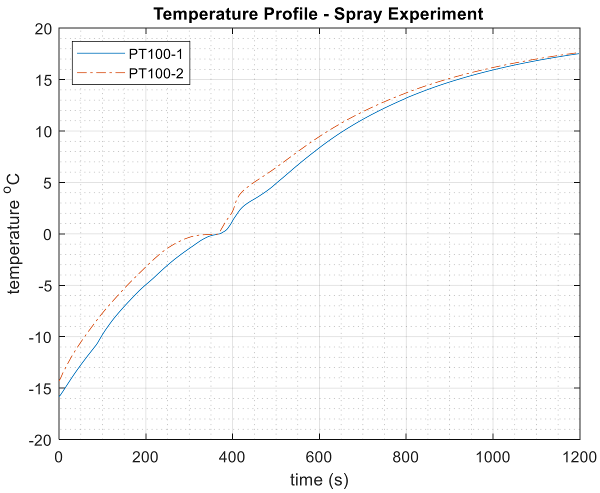


Figure 8. Temperature history for spray experiment.

A comparison of the derived $T$ parameter is shown in Figure 9. This represents two separate experiments with the aforementioned temperature profiles, but it is revealing to plot these on the same axes.

The trajectory of the dry apparatus is essentially linear along the real axis, with an approximately constant imaginary part. This is reasonable, since the attenuation would be approximately constant, although there would be some additional amplitude fluctuations due to the physical temperature itself affecting the received microwave signal, and hence the measured power along the real axis.

The spray case shows a somewhat different attenuation in relative terms. Importantly, the trajectory of the transmission measurement changes from liquid to ice.

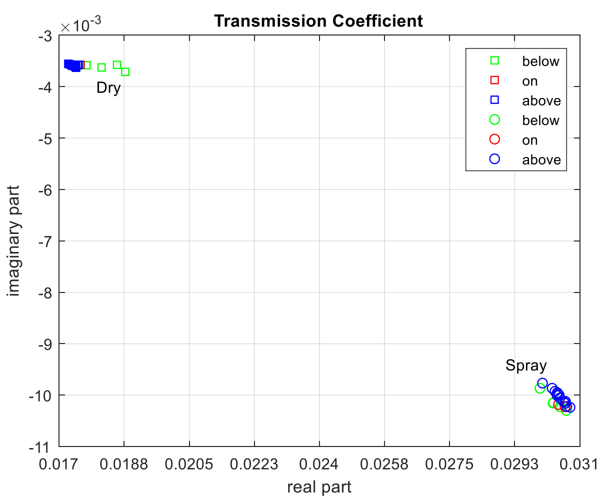


Figure 9. Transmission coefficient results for dry apparatus (upper left data – details presented in Figure x) and apparatus with approximately 0.8 g of spray (lower right data – details presented in Figure x). Results color-coded according to temperature: ‘below’ ($T < 0$ °C); ‘on’ ($T \approx 0$ °C); ‘above’ ($T > 0$ °C).

These two separate experiments as show in Figure 9 are shown individually in Figures 10 and 11. Figure 10 shows the approximately linear, horizontal trajectory along the real axis as noted previously for the dry apparatus case. Figure 11, for the < 1 g spray case, exhibits a trend not unlike the large-mass case. Note that the precise determination of the “transition” region is somewhat problematic, as the individual PT-100 sensors only determine a local temperature, and do not measure individual spray droplets. Nevertheless, the broad similarities are readily apparent. First, the localization of points in the dry case is not dissimilar. Secondly, the movement on the complex $T$ plane of the transition region exhibits similarities to the large-mass case, in that the attenuation and phase both show measurable differences over the temperature range and water state.

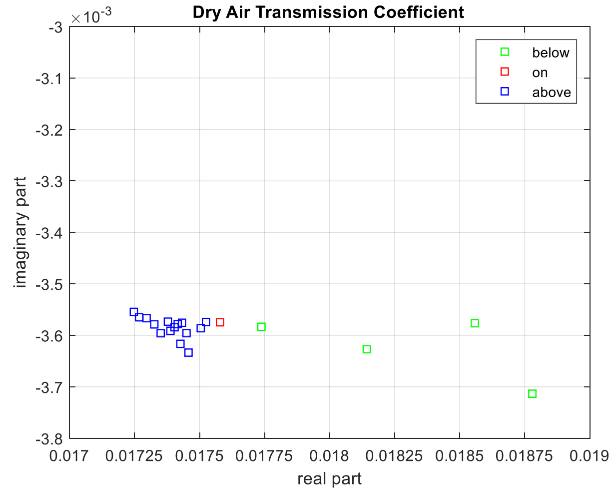


Figure 10. Transmission coefficient results for dry apparatus. Results color-coded according to temperature: ‘below’ ($T < 0$ °C); ‘on’ ($T \approx 0$ °C); ‘above’ ($T > 0$ °C).

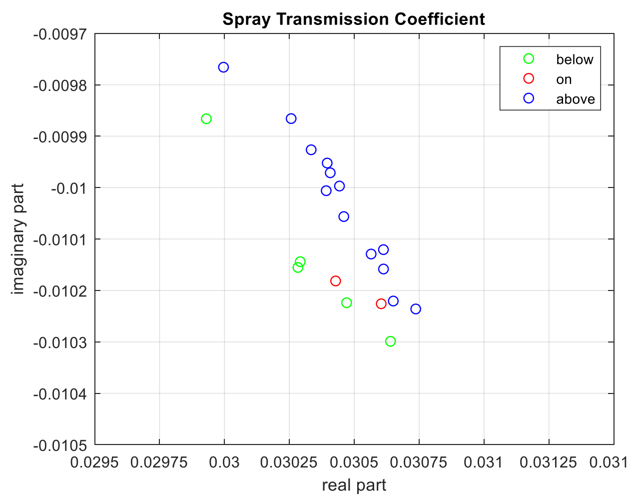


Figure 11. Transmission coefficient results for spray. Results color-coded according to temperature: ‘below’ ($T < 0$ °C); ‘on’ ($T \approx 0$ °C); ‘above’ ($T > 0$ °C).

# Conclusions

The measurement of material properties using electromagnetic (EM) waves has a long history in many domains. A passive approach is often used, in applications such as remote sensing. We propose herein the use of an active approach to the detection of liquid water. It is found that at high water concentrations, the presence of ice and the presence of liquid water are clearly delineated. Moreover, the transition region as determined from a thermal equilibrium approach may be mapped into the transmission parameter, which in turn is derived from the microwave scattering parameter measurements. Measurement of substantially smaller water quantities appears viable using this approach.

Several avenues for future research have become evident as a result of this work. First, improvements in the hardware including higher transmit powers and better transmit/receive antenna arrangements are desirable. The choice of several other parameters requires closer investigation – in particular, the choice of frequency band(s) and the resolution bandwidth, with a tradeoff being evident between processing time and measurement accuracy. Finally, the post-processing and algorithmic treatment of the measured data is critical. The VNA approach permits measurements over a frequency band, rather than a specific frequency, and this may be used to advantage to integrate the transmission profile, or alternatively to select highly active absorption regions for comparison with less active regions which can be used as a baseline reference.

## References


1. Currie, T. C., Fuleki, D., Knezevici, D. C. and MacLeod, J. D., "Altitude scaling of ice crystal accretion", 5th AIAA Atmospheric and Space Environments Conference, Fluid Dynamics and Co-located Conferences, AIAA 2013-2677, 2013.
2. Struk, P., Bartkus, T., Tsao, J.-C., Currie, T. and Fuleki, D., "Ice accretion measurements on an airfoil and wedge in mixed-phase conditions", SAE Technical Paper No. 2015-01-2116, 2015.
3. Davison, C., MacLeod, J. and Strapp, J., "Naturally aspirating isokinetic total water content probe: Evaporator design and testing", in 1st AIAA Atmospheric and Space Environments Conference, Fluid Dynamics and Co-located Conferences, AIAA 2009-3861, 2009, doi:10.2514/6.2009-3861.
4. Korolev, A.V., Strapp, J. W., Isaac, G. A., and Nevzorov, A. N., "The Nevzorov airborne hot-wire LWC-TWC probe: Principle of operation and performance characteristics," *Journal of Atmospheric and Oceanic Technology*, 15(6):1495–1510, 1998.
5. Korolev, A., Strapp, J., Isaac, G. and Emery, E., "Improved airborne hot-wire measurements of ice water content in clouds", *Journal of Atmospheric and Oceanic Technology*, 30(9):2121–2131, 2013
6. Hales, A., Quarini, G., Hilton, G., Ash, D., et al., "Ice fraction measurement of ice slurries through electromagnetic attenuation," *International Journal of Refrigeration*, 47:98–104, 2014.
7. Jean, B. R., "A microwave sensor for steam quality," *IEEE Transactions on Instrumentation and Measurement*, 57(4):751–754, 2008.
8. Trapp, T.J., Shannon, T.A., Herrera, B.J., Jean, B.R., McClain, S.T., "Electromagnetic Sensor for Detection of Ice Accretion inside Turbofan Jet Engines", 9th AIAA Atmospheric and Space Environments Conference, AIAA Aviation Forum, AIAA 2017-4248, 2017.
9. Faulkner, C.D., Herrera, B., Jean, B.R., and McClain, S.T., "Improved electromagnetic sensor for detection of ice accretion inside turbofan engine axial compressor stages," 2018 Atmospheric and Space Environments Conference, AIAA Aviation Forum, AIAA 2018-4226, 2018.
10. Nelson, S. and Kraszewski, A.W., "Grain moisture content determination by microwave measurements", *Transactions of the ASAE*, 33:1303-1305, 1990.
11. Artemov, V.G. and Volkov, A.A., "Water and ice dielectric spectra scaling at 0 °C," *Ferroelectrics*, 466(1): 158–165, 2014.
12. Matsuoka, T., Fujita, S., and Mae, S., "Effect of temperature on dielectric properties of ice in the range 5-39 GHz," *Journal of Applied Physics*, 80(10):5884–5890, 1996.
13. Rumiantsev, A. and Ridler, N., "VNA calibration," *IEEE Microwave Magazine*, 9(3):86–99, 2008.
14. Evans, J.G, "Measuring frequency characteristics of linear two-port networks automatically," *The Bell System Technical Journal*, 48(5):1313–1338, 1969.
15. Kruppa, W. and Sodomsky, K.F., "An explicit solution for the scattering parameters of a linear two-port measured with an imperfect test set (correspondence)," *IEEE Transactions on Microwave Theory and Techniques*, 19(1):122–123, 1971.
16. Nicolson, A. M. and Ross, G.F., "Measurement of the intrinsic properties of materials by time-domain techniques," *IEEE Transactions on Instrumentation and Measurement*, 19(4):377–382, 1970.
17. Weir, W.B., "Automatic measurement of complex dielectric constant and permeability at microwave frequencies," *Proceedings of the IEEE*, 62(1):33–36, 1974.
18. Digman, M.F., Conley, S. P., and Lauer, J. G., "Evaluation of a microwave resonator for predicting grain moisture independent of bulk density", *Applied Engineering in Agriculture*, 28(4):611-617, 2012.


## Contact Information

David Buttsworth, david.buttsworth@usq.edu.au